D406A钢焊接接头断裂韧度测试

邹吉权[1,2], 荆洪阳[1], 霍立兴[1]
(1. 天津大学 材料科学与工程学院, 天津 300072;
2. 天津职业大学 机电工程与自动化学院 300402)

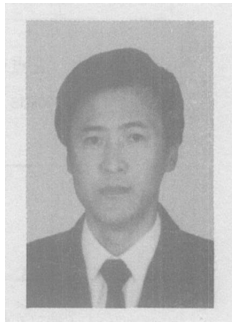

邹吉权

摘 要: 根据英国标准BS7448断裂韧度试验标准, 采用多试样法, 测试了D406A超高强度钢焊接接头的$J-R$曲线。取尺寸为B(板厚)×2B、缺口方向为板厚方向、带预制疲劳裂纹的标准试样进行三点弯曲试验。测试试件焊缝和热影响区的载荷—施力点位移曲线, 从而得到J积分。然后对数据点进行拟合得到$J-R$曲线, 计算出J积分临界值, 从而解决了由于板厚不足而无法直接测试焊接接头临界应力强度因子的问题, 为固体火箭发动机壳体设计提供依据。

关键词: 超高强度钢; 焊接接头; J积分; 阻力曲线
中图分类号: TG404 文献标识码: A 文章编号: 0253-360X(2006)11-091-04

0 序 言

随着空间技术的发展, 飞行器的发动机等高压容器都广泛采用了超高强度钢薄壁焊接结构, 但与此同时, 脆断事故时有发生[1]。研究表明, 这些脆断事故大多发生在焊接接头部位, 这是因为接头部位的组织、力学性能极不均匀, 并且可能存在气孔、夹渣、裂纹等缺陷。因此研究其接头部位的断裂性能具有重要的意义。

D406A钢是为固体火箭发动机壳体设计需要而研制的超高强度钢, 采用双真空冶炼(VIM+VAR), 其含碳量较低, 强度与韧性匹配合理。火箭发动机壳体采用焊接结构。该钢种母材的断裂韧度已有测试, 但焊接接头的断裂韧度的测试研究尚未见报导。

近几年, 英国焊接研究所提出了BS7448标准, 即"测定金属材料K_{IC}、极限COD和极限J积分值方法"[2], 该标准把K_{IC}、COD和J_{IC}三个断裂力学参量的测试统一起来, 受到了国际焊接学会的重视, 并予以推广应用。现已被国际标准局采纳[3]。文中的研究即采用英国标准BS7448 Part 4, 用J阻力曲线测得D406A钢焊接接头的弹塑性断裂参量$J_{0.2BL}$, 从而为固体火箭发动机壳体设计提供依据。

1 母材的化学成分与力学性能

母材的化学成分见表1, 力学性能见表2。

表1 D406A钢的化学成分(质量分数, %)
Table 1 Chemical composition of D406A steel

C	Si	Mn	Cr	Ni	Mo	V	S, P	Fe
0.29	1.66	0.85	1.10	0.25	0.44	0.09	≤0.01	余量

表2 D406A钢的力学性能
Table 2 Mechanical properties of D406A steel

屈服强度 R_{eL}/MPa	抗拉强度 R_m/MPa	断后伸长率 A(%)
1 320.0	1 643.0	9.5

2 试样制备

2.1 试样形状与尺寸及制备

采用三点弯曲标准试样(SENB), W/B名义上等于2, 裂纹长度a名义上等于厚度B, 并且在0.45~0.55 W之间。

试样尺寸取钢板原始厚度, 按原始厚度确定试样的尺寸。沿着钢板的轧制方向(纵向$L-T$)截取试样。试样形式如图1所示, 其中L为试件长度, S为跨距。

试样经最终热处理(930 ℃油淬, 300 ℃回火2 h[4])和精加工之后, 用线切割机制备疲劳裂纹引发缺口, 钼丝直径为0.12 mm。缺口位置如图2所示, 分别开在焊缝中心和热影响区, 热影响区缺口与熔合线在板厚中心相交[5]。

收稿日期: 2005-11-25

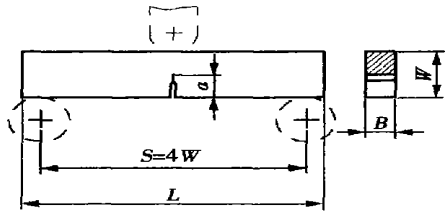

图 1 三点弯曲试样

Fig. 1 Three points bending specimen

(a) 缺口在焊缝中心

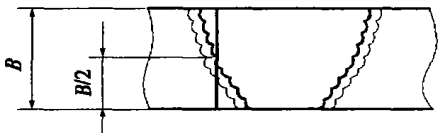

(b) 缺口在熔合线

图 2 缺口位置

Fig. 2 Notch location

在 10 t 高频疲劳试验机上，采用三点弯曲疲劳加载方式预制疲劳裂纹。按标准规定的方法分别测量试样厚度 B 和试样宽度 W。将预制好裂纹的试样粘贴刀口。

3 试验程序

安装好夹式引伸计，采用美国进口的 MTS880 万能材料试验机进行连续加载，加载速率为 1.0 mm/min，记录载荷—施力点位移（$F-s$）曲线。研究采用多试样法（7 个试样），分别加载到不同的裂纹扩展量。第一个试样加载到 $F-s$ 曲线达到最大载荷并刚刚开始下降时卸载。根据纪录的 $F-s$ 曲线，估计以后各试样加载终止的位移量。将试样卸载，并用热着色法勾出裂纹前缘。将试样压断，显示裂纹前缘。断口上平坦的预制裂纹前缘是裂纹稳定扩展的起点，热着色的终点为裂纹扩展的终止位置。观察断口形貌如图 3 所示，试样断口大部分为脆性断口。

用工具显微镜在断口上测定裂纹长度。按如图 4 所示的位置沿板厚分成 9 等份，分别测量这 9 个位置上的 Δa，取平均值。

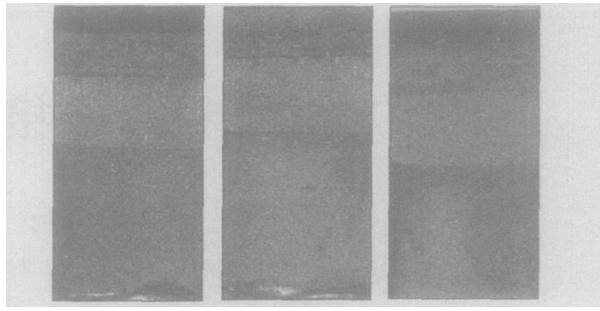

(a) (b) (c)

图 3 断口形貌

Fig. 3 Frecture image

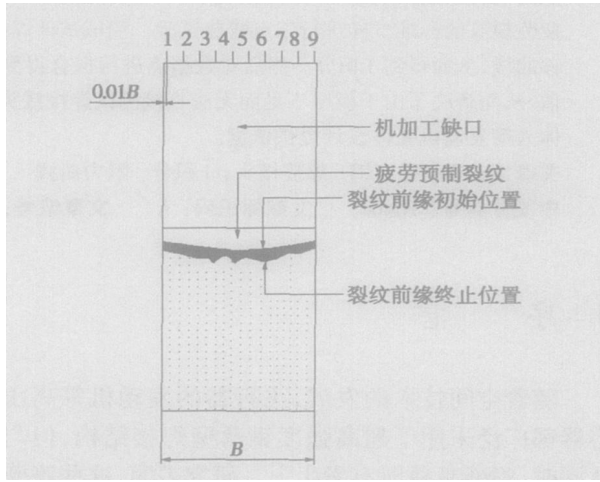

图 4 测量裂纹初始和终了长度

Fig. 4 Measure initial and final crack lengths

4 试验结果及数据处理

4.1 试验 $F-s$ 曲线

载荷—施力点位移曲线见图 5。

4.2 J 积分的计算

测得载荷—施力点位移（$F-s$）曲线后，用数值积分法求得 $F-s$ 曲线下的面积 A，即塑性功 U_p，如图 6 所示。

J 积分可由下式计算得出

$$J_{corr}=J_0\left(1-\frac{0.75\eta_p-1}{W-a}\Delta a\right),$$

式中：$J_0=\frac{K^2(1-\nu^2)}{E}+\frac{\eta_p U_p}{B(W-a_0)}$。

对于单边缺口弯曲试样，$\eta_p=2$

$$K=\frac{FS}{W^{1.5}B}\times g_1\left(\frac{a_0}{W}\right),$$

式中：F 为在试验期间施加的单调载荷；E 为弹性模量，取 2.1×10^5 MPa；ν 为泊松比，取 0.3；B 为板厚；W 为板宽；S 为跨距；$g_1(\alpha_0/W)$ 为试样几何形状系数。

J_{corr} 的计算的计算结果见表 3。

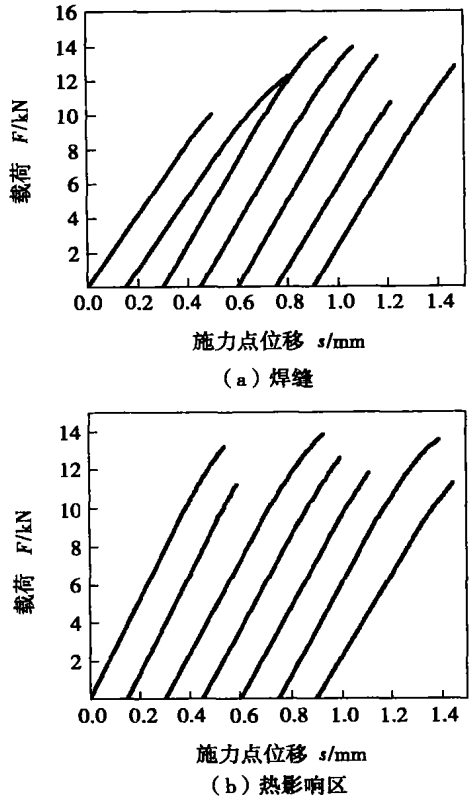

图 5　载荷—施力点位移曲线

Fig. 5　Force vs. displacement curves

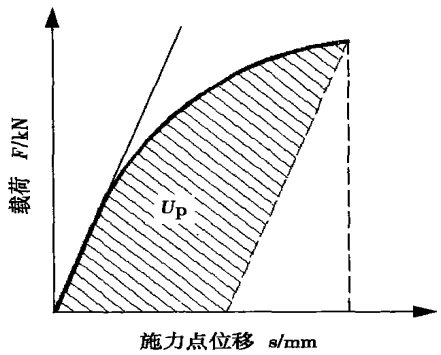

图 6　U_p 的确定

Fig. 6　Definition of U_p

5　$J-R$ 曲线的建立

5.1　做排除线

将测得的 J 值对裂纹扩展量 Δa 做图。裂纹扩展极限按式 $\Delta\alpha_{max}=0.10(W-a_0)$ 确定。根据试验数据画出钝化线。

$$J=3.75R_m\Delta a,$$

式中：R_m 为试验温度下的抗拉强度(MPa)。

表 3　试验结果

Table 3　Test results

	试样编号	裂纹长度 a/mm	裂纹扩展 Δa/mm	J 积分 J_{cor}/(N·mm^{-1})
热影响区	T—H—1	8.516	0.124	78.39
	T—H—2	8.338	0.250	93.25
	T—H—3	8.338	0.336	64.22
	T—H—4	8.396	0.41	56.18
	T—H—5	8.396	0.558	89.54
	T—H—6	8.338	0.664	61.04
	T—H—7	8.516	0.815	42.50
焊缝	T—W—1	8.326	0.121	51.47
	T—W—2	8.326	0.212	91.74
	T—W—3	8.614	0.324	86.63
	T—W—4	8.614	0.430	74.60
	T—W—5	8.582	0.520	65.38
	T—W—6	8.282	0.680	41.03
	T—W—7	8.282	0.820	63.85

5.2　曲线拟合

用下述方程对 $\Delta a=0.1$ mm 到 Δa_{max} 排除线之间的数据点拟合曲线

$$J=m+l(\Delta a)^x。$$

l, m, x 可按下述方法确定：

首先取从 0.01～1 之间的 x 值，间隔为 0.01，然后对每一个 x 值按下式计算矫正系数 r 为

$$r=\left[\sum J_i(\Delta a_i)^x-\frac{\sum\Delta a_i^x\sum J_i}{k}\right]\times\left\{\left[\sum J_i^2-\frac{(\sum J_i)^2}{k}\right]\left[\sum\Delta a_i^{2x}-\frac{(\sum\Delta a_i^x)^2}{k}\right]\right\}^{-0.5},$$

式中：k 为数据点的个数。

当 x 值具有最大矫正系数 r 时，可得出最佳拟合曲线。确定 x 值后，按下式分别计算 m 和 l 的值：

$$l=\left[\sum J_i^2-\frac{(\sum J_i)^2}{k}\right]^{0.5}\left[\sum\Delta a_i^{2x}-\frac{(\sum\Delta a_i^x)^2}{k}\right]^{-0.5}。$$

$$m=\frac{\sum J_i-l\sum\Delta a_i^x}{k}。$$

应当说明，l 和 m 的计算结果均应大于或等于 0，$0\leqslant x\leqslant 1$，如果 l 或 m 取负值，则应当补充试验数据点。

控制裂纹扩展的 J 极限值，分别用下述二式计算 J_{max} 值，并取二者较小值，即

$$J_{max}=(W-a_0)\frac{R_{P0.2}+R_m}{40},$$

$$J_{max}=B\left(\frac{R_{P0.2}+R_m}{40}\right),$$

式中：$R_{P0.2}$ 为延伸强度。

5.3 曲线拟合结果

最终分别得到焊缝和热影响区的 $J-R$ 曲线，如图 7 所示。偏置 0.2 mm 作钝化线的平行线，该线与拟合曲线的交点即 $J_{0.2BL}$。

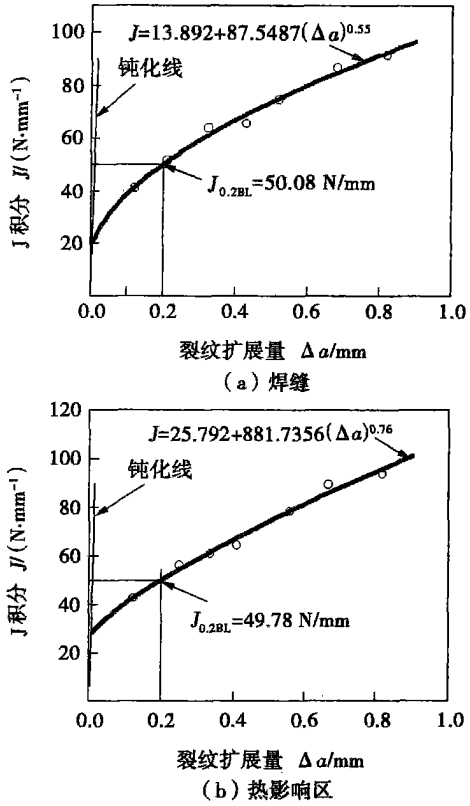

图 7 $J-R$ 曲线

Fig. 7 $J-$ Resistance curves

$J_{0.2BL}$ 表征从钝化线 0.2 mm 处断裂阻力参量，从工程角度讲，该处定义为启裂点，它表征启裂韧度。研究即采用 $J_{0.2BL}$ 作为材料的 J_{IC} 值。焊缝的 $J_{0.2BL}=50.08$ N/mm，热影响区的 $J_{0.2BL}=49.78$ N/mm。

6 结 论

（1）试验结果表明，焊缝和热影响区的 $J_{0.2BL}$ 值差别不大，并且都略大于母材的 $J_{0.2BL}$，说明焊接接头具有较好的抗开裂性能，所采用的焊接材料和焊接工艺是可行的。

（2）采用英国标准 BS7448 测得的 $J-R$ 阻力曲线可在小试样下测试材料的断裂韧度，解决了由于板厚太小而难以直接测试 K_{IC} 的问题。

参考文献：

[1] 汪德根，申辉旺. 高强度钢表面裂纹(K_{IC})的测定[J]. 钢铁，1995，30(9)：50—53.

[2] BS 7448：Part4，1997，Method for determination of fracture resistance curves and initiation values for stable crack extension in metallic materials[S].

[3] 霍立兴. 焊接结构的断裂行为及评定[M]. 北京：机械工业出版社，2000.

[4] 中华人民共和国国家军用标准，GJB3324—98，航天固体火箭发动机用超高强度钢板规范[S].

[5] BS 7448，Part2，1997，Fracture mechanics toughness tests. Method for determination of K_{IC}，critical CTOD and critical J values of welds in metallic materials[S].

作者简介：邹吉权，男，1965 年出生，博士研究生，副教授。主要研究方向为焊接结构的强度与断裂，已发表论文 7 篇。

Email：zoujiquan@eyou.com

Technology, Beijing 100022, China). p77—80

Abstract: The effects of different shielding gases CO_2, Ar and mixture gases (CO_2 + Ar) on the slag detachability of type 347L flux-cored wire for stainless steels containing Nb were investigated. Slag detachability of home-made GDQA347L (3 #) was compared with that of TFW-347L flux-cored wire and AT-Y347L flux-cored in the same condition. The effects of slag microstructure and macroscop on the slag detachability of three type flux-cored wires were investigated. The results showed that the best slag detachability of GDQA347L flux-cored wire was under the shielding gas of Ar; and the better slag detachability was under the shielding gas of mixture gas (CO_2 + Ar), and the worst slag detachability was under the shielding gas of CO_2. Because the CO_2 gas transfer into active gas at high temperature with strong oxidizability which will make detachment difficult on the slag detachability, and it is proved that the regular of microstructure of three flux-cored wires under different shielding gases is similar. It is benefit for the slag detachability when the trunk of the strip-shaped slag microstructure is long and the area of the branch is large.

Key words: type 347L flux-cored wire for stainless steels; slag detachability; shielding gas

Auto-adapting heat source model for numerical analysis of friction stir welding LI Hong-ke, SHI Qing-yu, ZHAO Hai-yan, LI Ting (Department of Mechanical Engineering, Tsinghua University, Key Laboratory for Advanced Materials Processing Technology, Ministry of Education, Beijing 100084, China). p81—85

Abstract: The heat generation mechanism and dependency of material properties on temperature can't be fully characterized by the heat source models used now. According to friction mechanics, a heat generation model based on yield strength was established. The model can make auto-adaptation to material property and temperature variation and represent the physical nature during FSW process. Comparison between experiment of thermal field and simulation results indicates that the accuracy is quite good for this new heat model.

Key words: friction stir welding; temperature field; heat source model; numerical simulation

Effect of electromagnetic stirring on microstructure and properties of surfacing metal CHENG Jiang-bo[1,2], XU Bin-shi[2], LIU Zheng-jun[3], WU Yi-xiong[1] (1. School of Material Science and Engineering, Shanghai Jiaotong University, Shanghai 200240, China; 2. RM of the Academy of Armored Forces Engineering, Beijing 100072, China; 3. School of Material Science and Engineering, Shenyang University of Technology, Shenyang 110023, China). p86—90

Abstract: The effect of electromagnetic stirring on the microstructure and properties of surfacing metal during the applied longitudinal intermittent alternative magnetic field on low carbon steel with plasma arc surfacing are investigated and discussed. The surfacing metal was analyzed using optical metallography, X-ray diffraction, microhardness testing and wet sand rubber wheel abrasion testing. It's found that the hard phases are increasing and distributing homogeneously in the surface of surfacing layer with changing magnetic parameters and the wear resistance of surfacing metal is increasing gradually. The optimal result is acquired when the magnetic parameters are 3 A, 10 Hz. The experimental results indicate that the optimal effect of grain refining can be gained with the proper magnetic parameters and electromagnetic stirring can control the morphology of hard phase in surfacing metal. The morphology of hard phases with strip and hexagon distribution without magnetic field are shifted to only hexagon alignment distribution with proper magnetic field, which it can improve the hardness and wear resistance of surfacing metal greatly.

Key words: electromagnetic stirring; plasma arc surfacing; longitudinal magnetic field

Fracture toughness tests of D406A steel welded joints ZOU Ji-quan[1,2], JING Hong-yang[1], HUO Li-xing[1] (1. School of Material Science & Engineering, Tianjin University, Tianjin 300072, China; 2. School of Electromechanical and Automation, Tianjin Professional College, Tianjin 300402, China). p91—94

Abstract: In accordance with the fracture toughness test standard of BS7448, *J-R* curve tests were conducted with multiple specimen with welded joints of D406A ultra-high strength steel. According to the standard, the specimen with prefabricated fatigue crack has a standard 3 points bending shape that has a rectangular section of $B \times 2B$ (B: specimen thickness) and notch orientation of thickness direction. The load and load-line displacement of weld and heat affected zone were tested, and the values of J integral were calculated. Finally, *J-R* curves and the critical value of J were obtained through the data points best fitted. Thus the problem of failure to test the critical stress intensity factor in welded joints directly by lack of thickness of specimen was coped with and the reliable evidence was offered for the design of solid propellant rocket engine.

Key words: ultra-high strength steel; welded joint; J integral; resistance curve

Evaluation of typical metal transfer modes for covered electrode WANG Bao[1,2], YANG Lin[1], WANG Yong[2] (1. Technology Center for Welding Consumables, North University of China, Taiyuan 030051, China; 2. Institute of Welding Materials, Taiyuan University of Technology, Taiyuan 030024, China). p95—98

Abstract: There are four basic metal transfer modes, globular droplet transfer, flux-wall guided transfer, explosive transfer and spray transfer for covered electrode. Photoelectrical oscillograph is traditionally employed to analyze arc voltage and welding current as two major electric parameters for the purpose of understanding the stability degree of a welding operation. Only the general characteristic of metal transfer can be qualitatively described and the quantitative analysis can't be carried out. Those parameters, such as probability density distributions of arc voltage, welding current and the da-